Eur. Phys. J. A (2016) **52**: 209
DOI 10.1140/epja/i2016-16209-8

THE EUROPEAN PHYSICAL JOURNAL A

Regular Article – Theoretical Physics

Electric multipole response of the halo nucleus ^{6}He

Jagjit Singh[1,2,a], L. Fortunato[1,2], A. Vitturi[1,2], and R. Chatterjee[3]

[1] Dipartimento di Fisica e Astronomia "G. Galilei", via Marzolo 8, I-35131 Padova, Italy
[2] INFN, Sezione di Padova, via Marzolo 8, I-35131 Padova, Italy
[3] Department of Physics, Indian Institute of Technology, Roorkee 247 667, India

Received: 12 April 2016 / Revised: 16 June 2016
Published online: 28 July 2016 – © Società Italiana di Fisica / Springer-Verlag 2016
Communicated by T. Duguet

Abstract. The role of different continuum components in the weakly bound nucleus ^{6}He is studied by coupling unbound *spd*-waves of ^{5}He by means of simple pairing contact-delta interaction. The results of our previous investigations in a model space containing only *p*-waves showed the collective nature of the ground state and allowed the calculation of the electric quadrupole transitions. We extend this simple model by including also *sd*-continuum neutron states and we investigate the electric monopole, dipole and octupole response of the system for transitions to the continuum, discussing the contribution of different configurations.

1 Introduction

Due to the recent developments in the radioactive beam facilities around the world, it is possible to explore new phenomena in unstable nuclei far from the line of stability. In the vicinity of the neutron drip line, a neutron halo is among the most interesting phenomena found in some unstable nuclei [1]. Typical two-neutron halo nuclei are ^{6}He [2] (system under study), ^{11}Li [1], ^{14}Be [3] and recently observed ^{22}C [4]. These two-neutron halo nuclei are referred as Borromean nuclei [5], when there is no bound state between a valence neutron and a core nucleus. Borromean nuclei typically have small two-neutron separation energy (S_{2n}). Due to diminishing half-lives and narrow production cross sections, the experimental analysis of these drip line systems is a challenging issue. In these weakly bound nuclear systems, the properties of the continuum states become progressively more and more fundamental to the nuclear structure and reactions. On the theoretical side the treatment of low breakup thresholds, responsible for strong coupling of bound and continuum states is the challenging issue. A low breakup threshold introduces many new features such as large spatial density distribution [1, 2], evolution of new magic numbers [6], a narrow momentum distribution [7] and at lower excitation energies strong concentration of electric dipole strength [8–11] in these systems. In this paper we study the electric multipole response of the well-established halo nucleus ^{6}He. Experimentally the higher excited states of ^{6}He are still under discussion and the features of resonance states are still not very clear. In the eighties, the $J_\pi = 0^+$ ground state and first excited $J_\pi = 2^+$ state at energy 1.797 MeV have been confirmed in numerous reactions [12, 13]. In the late nineties, the ^{6}Li(^{7}Li, ^{7}Be)^{6}He charge-exchange reaction has been studied at $E(^7\text{Li}) = 350$ MeV and transitions to the known $J_\pi = 0^+$ ground state and the $J_\pi = 2^+$ state at $E_x = 0.0$ and 1.8 MeV (weak) and three strong and broad resonances at $E_x \approx 5.6, 14.6$ and 23.3 MeV have been observed [14]. The strong resonances at $\sim$ 5.6 MeV and $\sim$ 14.6 MeV are interpreted as 2^+ and $(1, 2)^-$ resonances, respectively. Proton-neutron exchange reactions between two fast colliding nuclei produced resonant-like structures around 4 MeV [15] of width $\Gamma \sim 4$ MeV, as well as asymmetric bump at $\sim$ 5 MeV [16], and these structures are explained as dipole excitations compatible with oscillations of positively charged ^{4}He core against halo neutrons. Different mechanisms have also been proposed to explain this mode and this phenomenon is still under debate. More recently, the two-neutron transfer reaction $p(^8\text{He}, t)$ at the SPIRAL facility at 15.4 AMeV (GANIL, Caen), populated a much narrower 2^+ ($\Gamma = 1.6$ MeV) state and a $J = 1$ resonance ($\Gamma \sim 2$ MeV) of unassigned parity at energies 2.6 and 5.3 MeV, respectively [17]. It is worthwhile to mention that a very new reaction $^3\text{H}(\alpha, p\alpha)2n$ with a four-body exit channel, induced by the interaction of alpha-particles at energy of $E_\alpha = 67.2$ MeV, apparently shows the existence of ten resonant states [18]. The most part of these states are narrow resonances, as their total width is less than the energy of a resonance. Figure 1 presents

[a] e-mail: jsingh@pd.infn.it

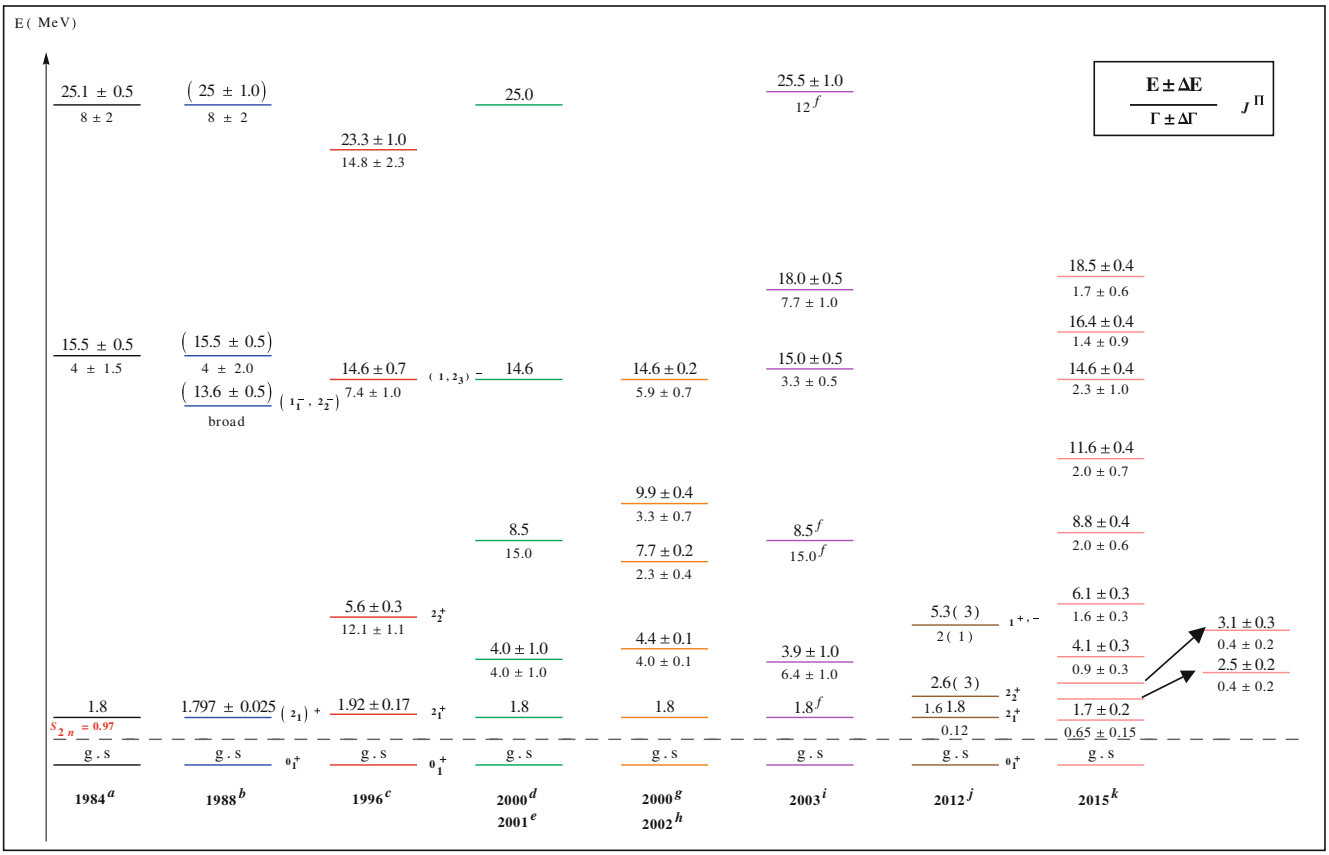

Fig. 1. (Color online) Experimental spectroscopy of ^{6}He. Notes: ^{a} Reference [12], (n,p) at 60 MeV/nucleon. ^{b} Reference [13]. ^{c} Reference [14], (^{7}Li, ^{7}Be) at 50 MeV/nucleon. ^{d,e} References [15, 19], (^{7}Li, ^{7}Be) at 65 MeV/nucleon. ^{g,h} References [16, 20], $(t, ^3$He) at 112 MeV/nucleon. ^{i} Reference [21], (^{7}Li, ^{7}Be t) at 65 MeV/nucleon. ^{j} Reference [17], (^{8}He, t) at 15.4 MeV/nucleon. ^{k} Reference [18], $(\alpha, p\alpha)$ at 67.2 MeV/nucleon. ^{f} Fixed in fits.

the chronological order of experimental data on ^{6}He. As it appears from this picture, there is no general consensus on the spectrum and the role of the continuum is far from being understood.

On the theoretical side, the $2n$-halo structure of ^{6}He was investigated in several different formalisms. Many predictions, most of which incomplete in one way or another, suggest a sequence of levels 0^+_{gs}, 2^+_1, 2^+_2, 1^+, 0^+_1, but disagree on the positions and widths of these states. Most of the ^{6}He structure predictions took only p-shell excitations into account, but more complete picture must include the promotion of neutrons to sd-shell. In particular sd-shell plays a vital role, allowing the possibility of dipole excitations to the continuum. The halo structure of ^{6}He is quite well understood by $^4\mathrm{He} + n + n$ model. The binding energy is underestimated by a small amount (~ 0.2 MeV less than the observed value) and this suggests that ^{4}He core excitations might be important [22–26]. In order to understand the weak binding characteristics of light nuclei close to the drip line, the continuum coupling effects have been investigated within various frameworks: the Gamow Shell model [27–30], the Continuum Shell Model [31], the Complex Scaled Cluster Orbital Shell Model [32] and the Hyperspherical Harmonics Expansion [5]. All these nuclear models are successful in predicting the ground state and first excited state structure to a reasonable degree, but they disagree for predictions of other higher excited states. The Quantum Monte Carlo p-shell calculations [33], along with well established ground state and first excited state structure, predict the energy of the excited 0^+ state at about 4.66 MeV, depending on the interaction used. In other calculations, the energy of the excited 0^+ state might be as low as 4.9 MeV [32] or as high as 8 MeV [29]. The energy of the 1^+ state covers the range of 3.4 [29] to 8 [34,35] MeV. On the other hand, in the few-body calculations of refs. [36, 37], the two 0^+ states were nearly pure jj-coupled states. This calculation allowed excitations into the sd-shell, but these turned out to be small for the g.s. and even less for the excited 0^+ state. The sd-shell occupancy was larger for the 2^+ states. In order to avoid the uncertainties due to the treatment of α particle as point particle, recently ref. [38] studied the ^{6}He nucleus in a fully microscopic six-nucleon calculation, claiming that the $E1$ strength function exhibits a two-peak structure at around 3 and 33 MeV excitation energy. The lower peak is well understood in the framework of the $\alpha + n + n$ structure and its excitation mechanism is consistent with the classical interpretation of the soft dipole mode (SDM). The higher peak is the typical giant dipole resonance that exhibits out-of-phase proton-neutron collective oscillations.

Just a few MeV above the SDM peak, some new modes are found that can be regarded as a vibrational excitation of the SDM. Most of the theoretical models explains ground-state structure fairly well to study dynamics of nuclear reactions, but they lack on incorporation of effects due to the presence of the continuum. These effects plays vital role to understand the major reason of their stable character. Only very recently in ref. [39] the continuum has been included, they found several resonances,including the well-known narrow 2_1^+ and the recently measured broader 2_2^+. Additional resonant states emerged in the $2^-$and 1^+ channels near the second 2^+ resonance and in the 0^- channel at slightly higher energy. Motivated by the recent experimental measurements at GANIL [17, 18], on continuum resonances in ^{6}He, we have developed a simple theoretical model [40] to study the weakly bound ground state and low-lying continuum states of ^{6}He by coupling two unbound p-waves of ^{5}He. In our approach, rather than simulating the resonance with a bound wave function, we calculate the full continuum single-particle spectrum of ^{5}He in a straightforward fashion and use two copies of the oscillating continuum wave functions to construct two-particle states. In the present study we have extended the model space with inclusion of *sd*-continuum waves of ^{5}He. The large basis set of these *spd*-continuum wave functions are used to construct the two-particle ^{6}He ground state 0^+ emerging from five different possible configurations, *i.e.* $(s_{1/2})^2$, $(p_{1/2})^2$, $(p_{3/2})^2$, $(d_{3/2})^2$ and $(d_{5/2})^2$. The simple pairing contact-delta interaction is used and pairing strength is adjusted to reproduce the bound ground state of ^{6}He. The extension of model space is a computationally challenging problem that required careful planning and consideration before undertaking the numerical work. The main aim is to show how an extension of theoretical concepts related to residual interactions, namely a contact delta pairing interaction, naturally explains the stable character of the bound states of Borromean nuclei, such as ^{6}He and simultaneously account for some of the resonant structures seen in the low-lying energy continuum. The extension of model space also allowed us to calculate the monopole, dipole and octupole response of the system.

The paper is organized as follows: sect. 2 describes the complete formulation of our simple structure model. In sect. 3 we analyzed the subsystem ^{5}He and sect. 4 presents a comparison of our present calculations on ground-state properties of ^{6}He with previous calculations. Section 5 describes the procedure that we have adopted for setting the pairing strengths for various multipolarities, followed by mathematical set up for electric transitions to continuum in sect. 6. Sections 7–9 presents the new results on monopole, dipole and octupole response of the system. Finally, sect. 10 presents our conclusions.

2 Model formulation

Each single-particle continuum wave function of ^{5}He is given by

$$\phi_{\ell,j,m}(\boldsymbol{r}, E_C) = \phi_{\ell,j}(r, E_C)\big[Y_{\ell m_\ell}(\Omega) \times \chi_{1/2,m_s}\big]^{(j)}_m. \quad (1)$$

We have used the midpoint method [41, 42] to discretize the continuum, in present calculations, which consists of taking the scattering state defined as

$$\tilde{\phi}_i(\boldsymbol{r}) = \sqrt{\Delta}\,\phi(\boldsymbol{r}, \bar{E}_i), \quad E_i > 0, \quad (2)$$

for a discrete set of scattering energies, where $\bar{E}_i = (E_i + E_{i-1})/2$, with Δ as common energy interval or width of the bin. In the midpoint method, continuum channels are represented by the channel at a midpoint of the bin. The resulting set of wave functions $\tilde{\phi}_{ij}(\boldsymbol{r})$ satisfies the following orthogonality condition:

$$\int \tilde{\phi}_i(\boldsymbol{r})\tilde{\phi}_j(\boldsymbol{r})\mathrm{d}\boldsymbol{r} = \Delta\,\delta_{ij}\delta(\bar{E}_i - \bar{E}_j), \quad (3)$$

that depends on the bin width (Δ). The combined tensor product of these two continuum states is given by

$$\psi_{JM}(\boldsymbol{r}_1, \boldsymbol{r}_2) = [\phi_{\ell_1,j_1,m_1}(\boldsymbol{r}_1, E_{C1}) \times \phi_{\ell_2,j_2,m_2}(\boldsymbol{r}_2, E_{C2})]^{(J)}_M. \quad (4)$$

In the following we will omit the explicit dependence on the energies E_{C1} and E_{C2}, although it is understood that each two-particle wave function still depends upon two energies. In LS-coupling the antisymmetric wave function $\psi(\ell_1\ell_2SLJM)$ is given by

$$\begin{aligned}\psi\,(\ell_1\ell_2SLJM) = {} & \frac{1}{\sqrt{1+\delta_{l1,l2}}} \\ & \times \sum_{M_S,M_L} \langle SM_SLM_L|SLJM\rangle \\ & \times \big[\phi_{12}(\ell_1\ell_2LM_L)\chi_{12}(s_1s_2SM_S) \\ & - \phi_{21}(\ell_2\ell_1LM_L)\chi_{21}(s_2s_1SM_S)\big]. \end{aligned} \quad (5)$$

By making use of symmetry relations eq. (5) can be written as

$$\begin{aligned}\psi\,(\ell_1\ell_2SLJM) = {} & \frac{1}{\sqrt{1+\delta_{l1,l2}}} \\ & \times \sum_{M_S,M_L} \langle SM_SLM_L|SLJM\rangle \\ & \times \big[\phi(\ell_1\ell_2LM_L) + (-1)^{(\ell_1+\ell_2-L+S)} \\ & \times \phi(\ell_2\ell_1LM_L)\big]\chi(s_1s_2SM_S). \end{aligned} \quad (6)$$

The generic matrix elements (diagonal and non-diagonal) due to mutual interaction V_{12} in LS-coupling of two particles are given by

$$\begin{aligned}&\langle \ell_a\ell_bSLJM|V_{12}|\ell_c\ell_dS'L'J'M'\rangle = \\ &\sum \langle SM_SLM_L|SLJM\rangle\langle S'M'_SL'M'_L|S'L'J'M'\rangle \\ &\times \langle s_1m_{s_1}s_2m_{s_2}|s_1s_2SM_S\rangle\langle s'_1m'_{s_1}s'_2m'_{s_2}|s'_1s'_2S'M'_S\rangle \\ &\times \langle \ell_am_a\ell_bm_b|\ell_a\ell_bLM_L\rangle\langle \ell_cm_c\ell_dm_d|\ell_c\ell_dL'M'_L\rangle \\ &\times \int \big[\phi_1(a)\chi_1(m_{s_1})\phi_2(b)\chi_2(m_{s_2})\big]^* V_{12} \\ &*\big[\phi_1(c)\chi_1(m'_{s_1})\phi_2(d)\chi_2(m'_{s_2})\big]\mathrm{d}\boldsymbol{r}_1\mathrm{d}\boldsymbol{r}_2, \end{aligned} \quad (7)$$

where quantum numbers ℓ_a and ℓ_c are associated with particle 1, ℓ_b and ℓ_d are associated with particle 2. ℓ_a and ℓ_b are coupled to L and ℓ_c and ℓ_d are coupled to L'. We take an attractive pairing contact delta interaction because we can reach the goal of calculation of electromagnetic response with only a few parameters (the pairing strengths). For $S = 0$ the explicit expression for V_{12} is given by

$$V_{12} = -g\delta\left(r_1 - r_2\right),$$

where

$$\delta\left(\boldsymbol{r_1} - \boldsymbol{r_2}\right) = \frac{\delta(r_1 - r_2)}{r_1 r_2}\delta\left(\cos(\theta_1) - \cos(\theta_2)\right)\delta\left(\varphi_1 - \varphi_2\right), \tag{8}$$

where g is the actual strength of the pairing interaction, is obtained by correcting the coefficient of the δ-contact matrix, G, with the energy spacing ΔE, *i.e.*

$$g = \frac{G}{(\Delta E)^2}. \tag{9}$$

Using eq. (1) and eq. (8) and making use of the fact that V_{12} is spin independent, the integral in eq. (7) can be rewritten as

$$\begin{aligned}
&\int \left[\phi_1(a)\chi_1(m_{s_1})\phi_2(b)\chi_2(m_{s_2})\right]^* V_{12} \\
&*\left[\phi_1(c)\chi_1(m'_{s_1})\phi_2(d)\chi_2(m'_{s_2})\right]\mathrm{d}\boldsymbol{r}_1\mathrm{d}\boldsymbol{r}_2 = \\
&\int R^*_{n_a\ell_a}(r)R^*_{n_b\ell_b}(r)\frac{1}{r^2}R_{n_c\ell_c}(r)R_{n_d\ell_d}(r)\mathrm{d}r \\
&\times \int Y^*_{\ell_a m_a}(\Omega)Y^*_{\ell_b m_b}(\Omega)Y_{\ell_c m_c}(\Omega)Y_{\ell_d m_d}(\Omega)\mathrm{d}\Omega,
\end{aligned} \tag{10}$$

where $R(r)$ are the radial parts of the scattering states defined in eq. (1). Using the property of two spherical harmonics of same angles, we have

$$\begin{aligned}
&\left[Y_{\ell_a m_a}(\Omega)Y_{\ell_b m_b}(\Omega)\right]^* = \sum_{\ell,m}(-1)^{\ell-m} \\
&\times \begin{pmatrix} \ell & \ell_a & \ell_b \\ -m & m_a & m_b \end{pmatrix}\langle\ell\|Y_{\ell_a}\|\ell_b\rangle^* Y_{\ell m}(\Omega)^*, \\
&\left[Y_{\ell_c m_c}(\Omega)Y_{\ell_d m_d}(\Omega)\right] = \sum_{\ell',m'}(-1)^{\ell'-m'} \\
&\times \begin{pmatrix} \ell' & \ell_c & \ell_d \\ -m' & m_c & m_d \end{pmatrix}\langle\ell'\|Y_{\ell_c}\|\ell_d\rangle Y_{\ell' m'}(\Omega),
\end{aligned} \tag{11}$$

where the Condon and Shortley phase convention has been adopted. Using the orthonormality property of spherical harmonics, we are left with

$$\begin{aligned}
&\int Y^*_{\ell_a m_a}(\Omega)Y^*_{\ell_b m_b}(\Omega)Y_{\ell_c m_c}(\Omega)Y_{\ell_d m_d}(\Omega)\mathrm{d}\Omega = \\
&\sum_{\ell,m}(-1)^{2(\ell-m)}\begin{pmatrix} \ell & \ell_a & \ell_b \\ -m & m_a & m_b \end{pmatrix}\begin{pmatrix} \ell & \ell_c & \ell_d \\ -m & m_c & m_d \end{pmatrix} \\
&\times\langle\ell\|Y_{\ell_a}\|\ell_b\rangle^*\langle\ell'\|Y_{\ell_c}\|\ell_d\rangle.
\end{aligned} \tag{12}$$

Hence, using the above assumptions and properties, eq. (7) is reduced to

$$\begin{aligned}
&\langle\ell_a\ell_b SLJM|V_{12}|\ell_c\ell_d S'L'J'M'\rangle = \\
&\sum\langle SM_S LM_L|SLJM\rangle\langle S'M'_S L'M'_L|S'L'J'M'\rangle \\
&\times\langle s_1 m_{s_1} s_2 m_{s_2}|s_1 s_2 SM_S\rangle\langle s'_1 m'_{s_1} s'_2 m'_{s_2}|s'_1 s'_2 S'M'_S\rangle \\
&\times\langle\ell_a m_a \ell_b m_b|\ell_a\ell_b LM_L\rangle\langle\ell_c m_c \ell_d m_d|\ell_c\ell_d L'M'_L\rangle \\
&\times\sum_{\ell m}(-1)^{2(\ell-m)}\begin{pmatrix} \ell & \ell_a & \ell_b \\ -m & m_a & m_b \end{pmatrix}\begin{pmatrix} \ell & \ell_c & \ell_d \\ -m & m_c & m_d \end{pmatrix} \\
&\times\langle\ell\|Y_{\ell_a}\|\ell_b\rangle^*\langle\ell'\|Y_{\ell_c}\|\ell_d\rangle \\
&\times\int R^*_{n_a\ell_a}(r)R^*_{n_b\ell_b}(r)\frac{1}{r^2}R_{n_c\ell_c}(r)R_{n_d\ell_d}(r)\mathrm{d}r.
\end{aligned} \tag{13}$$

The major ingredients for the complete study of ^{6}He are the matrix elements of pairing interaction. These correspond to the radial integrals and to the coefficients. The coefficients of these matrix elements of eq. (13) for 0^+, 1^-, 2^+ and 3^- are summarized in tables of [43]. The full computational procedure is described in details in [43,44].

3 Analysis of ^{4}He + n subsystem

An analysis of the $^4\mathrm{He} + n$ subsystem (^{5}He) is indispensable in studying ^{6}He as a typical nucleus of a Borromean system of $^4\mathrm{He}+n+n$. In order to study the binding mechanism of ^{6}He, the interaction between a core of ^{4}He and a valence neutron plays an important role. The unbound nucleus ^{5}He can be described as an inert ^{4}He core with an unbound neutron moving in p, d or s states in a simple independent-particle shell model picture. These p and d states are split by spin-orbit interaction. Experimentally only the $p_{3/2}$ and $p_{1/2}$ resonances are confirmed at 0.789 and 1.27 MeV, respectively above the neutron separation threshold. Their widths are quoted as 0.648 MeV and 5.57 MeV, respectively [45]. Theoretically in order to extend the model space we have also included the *sd*-shell in the picture. The continuum monopole ($\ell = 0$), dipole ($\ell = 1$) and quadrupole ($\ell = 2$) scattering single-particle states ($E_C > 0$, $k > 0$) of ^{5}He are generated with Woods-Saxon (WS) potential given by

$$V_{WS} = \left[V_0 + V_{ls}r_0^2(\vec{l}\cdot\vec{s})\frac{1}{r}\frac{\mathrm{d}}{\mathrm{d}r}\right]\left[1 + \exp\left(\frac{r_0 - R}{a}\right)\right]^{-1}, \tag{14}$$

where $R = r_0 A^{\frac{1}{3}}$. For ^{5}He the parameter set used is WS potential depth $V_0 = -42.6$ MeV, $r_0 = 1.2$ fm, $a = 0.9$ fm and spin-orbit coefficient $V_{ls} = 8.5$ MeV. The continuum single-particle wave functions are calculated (see fig. 2 of [40], fig. 1 of [43] and fig. 2 of [46]), with energies from 0.0 to 10.0 MeV, normalized to a Dirac delta in energy, for the *spd*-states of ^{5}He on a radial grid that goes from 0.1 fm to 100.0 fm with the potential given above.

4 Ground-state properties of ^{6}He

The simple model with two non-interacting particles in the above single-particle levels of ^{5}He produces different parity states (see table 1 of [46]) when two neutrons are placed in five different unbound orbits, $s_{1/2}$, $p_{1/2}$, $p_{3/2}$, $d_{3/2}$ and $d_{5/2}$. Namely five configurations $(s_{1/2})^2$, $(p_{1/2})^2$, $(p_{3/2})^2$, $(d_{3/2})^2$ and $(d_{5/2})^2$ couple to $J = 0^+$, seven configurations $(s_{1/2}d_{3/2})$, $(s_{1/2}d_{5/2})$, $(p_{1/2}p_{3/2})$, $(p_{3/2}p_{3/2})$, $(d_{3/2}d_{3/2})$, $(d_{3/2}d_{5/2})$ and $(d_{5/2}d_{5/2})$ couple to $J = 2^+$, five configurations $(s_{1/2}p_{1/2})$, $(s_{1/2}p_{3/2})$, $(p_{1/2}d_{3/2})$, $(p_{3/2}d_{3/2})$ and $(p_{3/2}d_{5/2})$ couple to $J = 1^-$ and three configurations $(p_{1/2}d_{5/2})$, $(p_{3/2}d_{3/2})$ and $(p_{3/2}d_{5/2})$ couple to $J = 3^-$. Other less important multipolarities can also be constructed as in table 1 of [46].

An attractive pairing contact delta interaction has been used, $-g\delta(\boldsymbol{r}_1 - \boldsymbol{r}_2)$ for simplicity, because we can reach the goal with only one parameter adjustment. With continuum single-particle wave functions, using the midpoint method with an energy spacing of 2.0, 1.0, 0.5, 0.2 and 0.1 MeV, corresponding to block basis dimensions of $N = 5$, 10, 20, 50 and 100, respectively, the two-particle states are formed and the matrix elements of the pairing interaction are calculated. The resulting matrix has been diagonalized with standard routines and it has given the eigenvalues shown in fig. 2 of [46] for the $J = 0^+$ case. It is clear from the eigenspectrum that, with increase in basis dimensions the superfluous bound state moves into the continuum. This was not present in our old work [40], and it can be attributed to the new, more complete basis. The coefficient of the δ-contact matrix, G, has been adjusted to reproduce the correct ground-state energy each time. The actual pairing interaction g is obtained by correcting with a factor that depends on the aforementioned spacing between energy states and it is practically a constant, except for the smallest basis. The biggest adopted basis size gives a fairly dense continuum in the region of interest. The radial part of the $S = 0$ g.s. wave function (see fig. 3 of [46]) obtained from the diagonalization in the largest basis, shows a certain degree of collectivity, taking contributions of comparable magnitude from several basis states, while in contrast the remaining unbound states usually are made up of a few major components [44]. The detailed components for each configuration are summarized in table 1, and compared with the previous calculations of Hagino [47] and Myo [48]. The present calculations are well in agreement with the previous calculations of Hagino and Myo, where Hagino [47] employed a simple three-body model by using the density-dependent contact interaction to calculate the ground state of ^{6}He and Myo [48] employed the complex scaled-cluster orbital shell model (CS-COSM) with the Minnesota interaction to fix the ground state of ^{6}He. The calculated ground-state properties are summarized in table 2 in comparison with calculations [47,48], where R_m is the matter radius,

$$\langle r_{NN}^2 \rangle = \langle \psi_{gs}(\boldsymbol{r}_1, \boldsymbol{r}_2) | (\boldsymbol{r}_1 - \boldsymbol{r}_2)^2 | \psi_{gs}(\boldsymbol{r}_1, \boldsymbol{r}_2) \rangle \quad (15)$$

is the mean square distance between the valence neutrons, and

$$\langle r_{c-NN}^2 \rangle = \langle \psi_{gs}(\boldsymbol{r}_1, \boldsymbol{r}_2) | (\boldsymbol{r}_1 + \boldsymbol{r}_2)^2/4 | \psi_{gs}(\boldsymbol{r}_1, \boldsymbol{r}_2) \rangle \quad (16)$$

is the mean square distance of their centre of mass with respect to the core. In table 2, while the matter radius is consistent with that of Myo, there are large differences for the other two quantities that can be ascribed to the choice of different pairing interactions. The two-particle density of ^{6}He as a function of two radial coordinates, r_1 and r_2, for valence neutrons, and of the angle between them, θ_{12}, in the LS-coupling scheme, is given by

$$\rho(r_1, r_2, \theta_{12}) = \rho^{S=0}(r_1, r_2, \theta_{12}) + \rho^{S=1}(r_1, r_2, \theta_{12}). \quad (17)$$

The explicit expression for $S = 0$ component is given by [49]

$$\rho^{S=0}(r_1, r_2, \theta_{12}) = \frac{1}{8\pi} \sum_L \sum_{\ell,j} \sum_{\ell',j'} \frac{\hat{\ell}\hat{\ell}'\hat{L}}{\sqrt{4\pi}} \begin{pmatrix} \ell & \ell' & L \\ 0 & 0 & 0 \end{pmatrix}^2 \times \psi_{\ell j}(r_1, r_2) \psi_{\ell' j'}(r_1, r_2) Y_{L0}(\theta_{12}) \times (-1)^{\ell+\ell'} \sqrt{\frac{2j+1}{2\ell+1}} \sqrt{\frac{2j'+1}{2\ell'+1}}, \quad (18)$$

where $\hat{\ell} = \sqrt{2l+1}$ and $\psi_{\ell j}(r_1, r_2)$ is the radial part of the two-particle wave function given by

$$\psi_{\ell j}(r_1, r_2) = \sum_{n2 \le n1} \frac{\alpha_{n_1 n_2 \ell j}}{\sqrt{2(1+\delta_{n_1 n_2})}} \times (\phi_{n_1 \ell j}(r_1)\phi_{n_2 \ell j}(r_2) + \phi_{n_1 \ell j}(r_2)\phi_{n_2 \ell j}(r_1)), \quad (19)$$

where n_1 and n_2 are radial quantum numbers and $\alpha_{n_1 n_2 \ell j}$ is an expansion coefficient. Figure 2 shows the two-particle density plotted as a function of the radius $r_1 = r_2 \equiv r$ and the angle θ_{12}, and with a weight factor of $4\pi r^2 \cdot 2\pi r^2 \sin\theta_{12}$. As has been pointed out in [47], one observes two peaks in the two-particle densities. The peaks at smaller and larger

Table 1. Components of the ground state (0_1^+) of ^{6}He.

Config.	Present	T. Myo [48]	Hagino [47]
$(2s_{1/2})^2$	0.008	0.009	–
$(1p_{1/2})^2$	0.080	0.043	–
$(1p_{3/2})^2$	0.897	0.917	0.830
$(1d_{3/2})^2$	0.005	0.007	–
$(1d_{5/2})^2$	0.009	0.024	–

Table 2. Radial properties of the ground state of ^{6}He in units of fm.

	Present	T. Myo [48]	Hagino [47]
R_m	2.37674	2.37	...
r_{NN}^2	28.8404	23.2324	21.3
r_{c-2N}^2	7.21011	9.9225	13.2

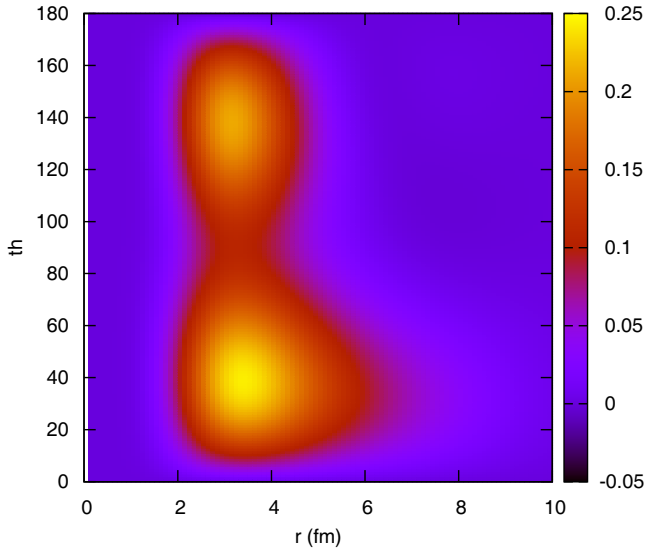

Fig. 2. (Color online) Two-particle density for ^{6}He as a function of $r_1 = r_2 = r$ and angle between the valence neutrons θ_{12}.

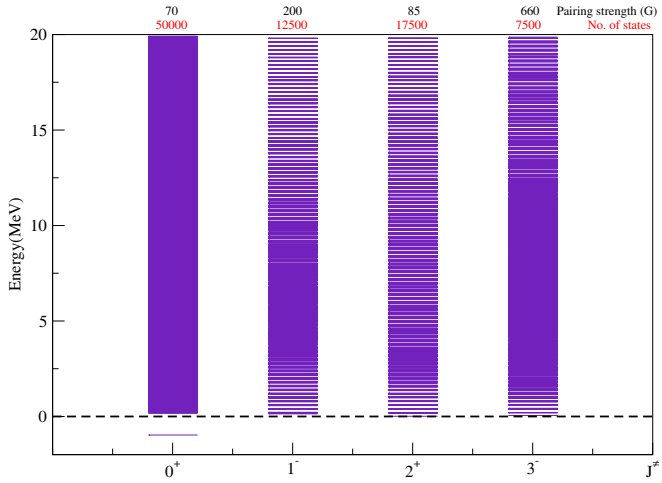

Fig. 3. (Color online) Eigenspectrum of the interacting two-particle case for $J^\pi = 0^+$, 1^-, 2^+ and 3^- for different number of states. The coefficient of the δ-contact matrix, G, has also been shown for different J.

θ_{12} are referred to as "di-neutron" and "cigar-like" configurations, respectively. In this case the di-neutron component has a slightly higher density and it has a longer radial tail, which confirms the halo structure of ^{6}He, while the cigar-like component has a very compact structure comparatively. The percentage contribution of di-neutron configuration is $\sim 64\%$, while the cigar component has $\sim 36\%$ contribution.

5 Pairing strength of different multipolarities

Theoretical investigation of very weakly bound nuclei sitting right on top of the drip lines demands proper consideration of nucleon-nucleon pairing interaction. For ground state it is pretty much clear that, the pairing strength, G, is adjusted in order to get the correct ground-state energy. But for higher multipolarities, *i.e.* $J = 1^-$, 2^+ and 3^-, we do not have a clear-cut strategy to determine the exact value of pairing strength. This is the main reason why we did not enter into the complications of a density-dependent pairing interaction: there is no unique way to adjust the parameters and geometry. For each value of J we tried different sets of values of G. From fig. 3, the upper limit of pairing strength can be found for several values of J, along with the number of states (red). Notice that different multipolarities give rise to different concentrations of strength as seen by comparing the densities of the various columns. Notice also that the continua are, at the eyes, quite dense, a condition that is necessary to reproduce minute features with the necessary accuracy.

Table 3. Effective charge for different multipolarities.

λ	$(e_{eff}^{(\lambda)})^2$
0 (Monopole)	4
1 (Dipole)	4/25
2 (Quadrupole)	4/625
3 (Octupole)	4/15625

6 Electric transitions to continuum —Mathematical set up

The electric transition probability amplitude between ground state $\psi(j_1', j_2', J', M')$ and continuum states $\psi(j_1, j_2, J, M)$ is given by

$$\langle\psi(j_1', j_2', J', M')|\hat{O}_p|\psi(j_1, j_2, J, M)\rangle =$$
$$\sum_{S',L'} \sqrt{(2S'+1)(2L'+1)(2j_1'+1)(2j_2'+1)} \begin{Bmatrix} 1/2 & \ell_1' & j_1' \\ 1/2 & \ell_2' & j_2' \\ S' & L' & J' \end{Bmatrix}$$
$$\times \sum_{S,L} \sqrt{(2S+1)(2L+1)(2j_1+1)(2j_2+1)} \begin{Bmatrix} 1/2 & \ell_1 & j_1 \\ 1/2 & \ell_2 & j_2 \\ S & L & J \end{Bmatrix}$$
$$\times\Big([\langle R^+_{\ell_1'\ell_2'}(r_1r_2)\Upsilon^+_{L'M'}(\Omega_1\Omega_2)|\hat{O}_p|R^+_{\ell_1\ell_2}(r_1r_2)\Upsilon^+_{LM}(\Omega_1\Omega_2)\rangle] + [\langle R^-_{\ell_1'\ell_2'}(r_1r_2)\Upsilon^-_{L'M'}(\Omega_1\Omega_2)|\hat{O}_p| \times R^-_{\ell_1\ell_2}(r_1r_2)\Upsilon^-_{LM}(\Omega_1\Omega_2)\rangle]\Big), \quad (20)$$

where $\hat{O}_p$ is a generic one-body operator given by

$$\hat{O}_p = e_{eff}^{(\lambda)}\left(r_1^\lambda Y_{\lambda\mu}(\hat{r}_1) + r_2^\lambda Y_{\lambda\mu}(\hat{r}_2)\right) \quad (21)$$

with $\lambda = 1$ for dipole, $\lambda = 2$ for quadrupole and $\lambda = 3$ for octupole, $e_{eff}^{(\lambda)}$ is the effective charge, tabulated in table 3 for different multipolarities and is given by

$$e_{eff}^{(\lambda)} = \frac{A_1^\lambda Z_2 + (-1)^\lambda A_2^\lambda Z_1}{A^\lambda}, \quad (22)$$

where we use the masses and charges of the α-particle and of a neutron for 1, 2 because the one-body operator acts only on one particle at any one time. Using eq. (21), eq. (20) can be rewritten as

$$\begin{aligned}
&\langle\psi(j_1',j_2',J',M')|\hat{O}_p|\psi(j_1,j_2,J,M)\rangle = \\
&\sum_{S',L'}\sqrt{(2S'+1)(2L'+1)(2j_1'+1)(2j_2'+1)}\begin{Bmatrix}1/2 & \ell_1' & j_1'\\ 1/2 & \ell_2' & j_2'\\ S' & L' & J'\end{Bmatrix}\\
&\times\sum_{S,L}\sqrt{(2S+1)(2L+1)(2j_1+1)(2j_2+1)}\begin{Bmatrix}1/2 & \ell_1 & j_1\\ 1/2 & \ell_2 & j_2\\ S & L & J\end{Bmatrix}\\
&\times 2\Bigg(\iint R^{+}_{\ell_1'\ell_2'}(r_1r_2)r_1^{\lambda}R^{+}_{\ell_1\ell_2}(r_1r_2)r_1^2\mathrm{d}r_1r_2^2\mathrm{d}r_2\\
&\times\langle\Upsilon^{+}_{L'M'}(\Omega_1\Omega_2)|Y_{\lambda\mu}(\Omega_1)|\Upsilon^{+}_{LM}(\Omega_1\Omega_2)\rangle\\
&+\iint R^{-}_{\ell_1'\ell_2'}(r_1r_2)r_1^{\lambda}R^{-}_{\ell_1\ell_2}(r_1r_2)r_1^2\mathrm{d}r_1r_2^2\mathrm{d}r_2\\
&\times\langle\Upsilon^{-}_{L'M'}(\Omega_1\Omega_2)|Y_{\lambda\mu}(\Omega_1)|\Upsilon^{-}_{LM}(\Omega_1\Omega_2)\rangle\Bigg). \qquad (23)
\end{aligned}$$

Also $R^{\pm}_{\ell_1'\ell_2'}(r_1r_2)$ and $\Upsilon^{\pm}_{L'M'}$ are given by

$$\begin{aligned}
R^{\pm}_{\ell_1\ell_2}(r_1r_2) &= \frac{1}{r_1r_2\sqrt{2}}\\
&\times\left[R_{n_1\ell_1}(r_1)R_{n_2\ell_2}(r_2)\pm R_{n_2\ell_2}(r_1)R_{n_1\ell_1}(r_2)\right], \qquad (24)
\end{aligned}$$

$$\begin{aligned}
\Upsilon^{\pm}_{LM} &= \frac{1}{\sqrt{2}}\sum\langle\ell_1m_1\ell_2m_2|\ell_1\ell_2LM\rangle\\
&\times\left[Y_{\ell_1m_1}(\Omega_1)Y\ell_2m_2(\Omega_2)\pm Y_{\ell_2m_2}(\Omega_1)Y_{\ell_1m_1}(\Omega_2)\right]. \qquad (25)
\end{aligned}$$

Using eq. (24) and eq. (25), eq. (23) gives us the matrix elements of different multipolarities. Equation (23) consists of two parts, *i.e.* evaluation of radial parts and angular parts. For the evaluation of radial integrals, we need the corresponding two-particle wave function, whereas for the angular part by making use of eq. (25), we will simplify the angular part and for different multipolarities these can be easily calculated.

Clearly our calculations give strength distributions at discrete values of energy to which we apply a Gaussian smoothing procedure that does not alter the total integrated strength[1].

7 Monopole strength distribution

Electric monopole transition strengths reflect the off diagonal matrix elements of the $E0$ operator. The $E0$ operator [50] can be expressed in terms of single-nucleon degrees of freedom as

$$\hat{T}(E0) = \sum_k e_k r_k^2. \qquad (26)$$

[1] There is a minor loss of strength close to zero that could be avoided by using for example Lorentzian functions instead of Gaussians.

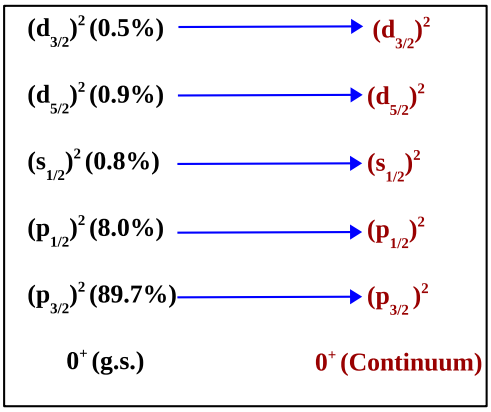

Fig. 4. (Color online) Total number of possible monopole transitions from the ground state 0^+ to the final continuum 0^+ states with different contributions from five different possible configurations for ^{6}He.

The $E0$ transition rate, $1/\tau(E0) = \rho^2_{fi}$, is defined by

$$\rho^2_{fi} = \left|\frac{\langle f|\sum_k e_k r_k^2|i\rangle}{eR^2}\right|^2, \qquad (27)$$

where, e is the unit of electrical charge, and R is the nuclear radius, $R \backsimeq 1.2A^{1/3}$ fm. These calculations also leads us to study the role of various configurations in the total monopole strength. After constructing a basis of the largest size ($N = 100$) made up of five parts, namely $[s^2_{1/2}]^{(0)}$, $[p^2_{1/2}]^{(0)}$, $[p^2_{3/2}]^{(0)}$, $[d^2_{3/2}]^{(0)}$ and $[d^2_{5/2}]^{(0)}$, we diagonalize the pairing matrix and obtain eigenvalues and eigenvectors for $J = 0$. Only one state is bound and all the remaining ones are unbound. In order to reduce the computation time, we have performed a set of calculations for monopole transitions from the ground state 0^+ for basis size $N = 100$ to the continuum 0^+ for basis size $N = 50$. From fig. 4, it is clear that there are only five possible transitions from 0^+ ground-state components to continuum 0^+ states components. With all these necessary ingredients, *i.e.* ground state and continuum 0^+ states, the monopole strength distribution has been studied. The upper panel of fig. 5, shows the total monopole transition strength of ^{6}He and lower panel of fig. 5, shows the contribution of various possible transitions on logarithmic scale. From the lower panel of fig. 5, it is clear that the transition $[(p_{3/2})^2]^{(0)}$(g.s.) $\rightarrow$ $[(p_{3/2})^2]^{(0)}$(continuum), is dominant in the monopole transition strength, whereas the transition $[(d_{3/2})^2]^{(0)}$(g.s.) $\rightarrow$ $[(d_{3/2})^2]^{(0)}$(continuum) is the least significant in the total monopole transition strength. From this, one can also see that the transition $[(s_{1/2})^2]^{(0)}$(g.s.) $\rightarrow$ $[(s_{1/2})^2]^{(0)}$(continuum) has a significant contribution to the total strength, which justifies the inclusion of the *sd*-shell in calculations. The total integrated monopole strength amounts to about 2682.97 fm^4. This value can be compared with the non-energy–weighted sum rule calculations for monopole strength, that gives about 2800 fm^4, using formulas of ref. [51], giving a very good agreement.

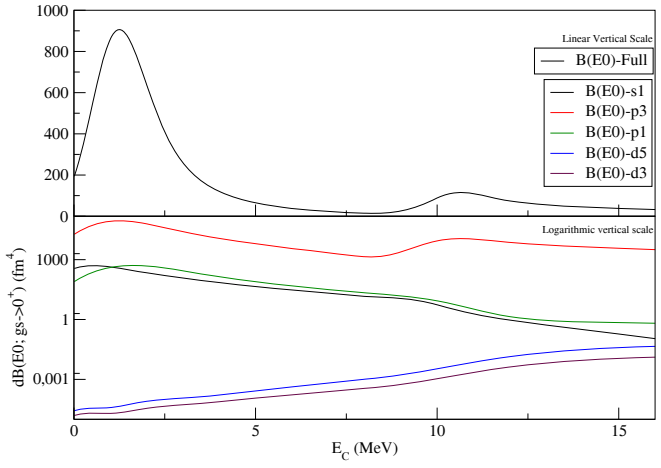

Fig. 5. (Color online) (Upper panel) Total monopole $E0$ transition strength distribution (on linear vertical scale) from ground state 0^+ to the final state 0^+ for ^{6}He. (Lower panel) Component monopole $E0$ transition strength distribution (on logarithmic vertical scale) from the ground state 0^+ to the final state 0^+ for ^{6}He.

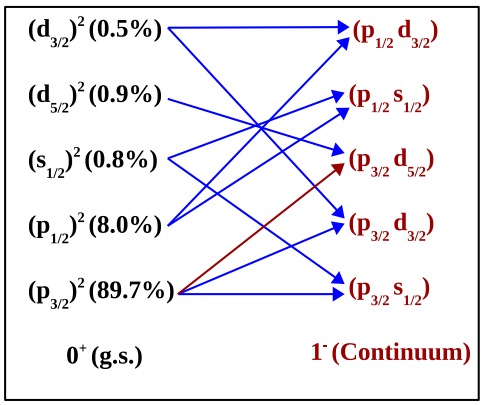

Fig. 6. (Color online) Total number of possible dipole transitions from the ground state 0^+ to the final state 1^- with different contributions from five different possible configurations for ^{6}He. The dominant transition is highlighted in red color.

8 Dipole strength distribution

While most theoretical studies have been focused on dipole strength [38,52,53], ours includes many more multipolarities. In order to compare our approach with others, we have also performed a set of calculations for the dipole response from the ground state to all components of 1^- state. After constructing a basis of the dimensions $N = 50$, made up of five parts, namely $[s_{1/2} \times p_{1/2}]^{(1)}$, $[s_{1/2} \times p_{3/2}]^{(1)}$, $[p_{1/2} \times d_{3/2}]^{(1)}$, $[p_{3/2} \times d_{3/2}]^{(1)}$ and $[p_{3/2} \times d_{5/2}]^{(1)}$, we diagonalize the pairing matrix and obtain eigenvalues, that are all unbound, and the corresponding eigenvectors. We did calculations for three different values of the pairing strength G, *i.e.* 0, 100 and 200 (upper limit to get all states unbound). From fig. 6, it is clear that a total of 10 different transitions are possible from the initial 0^+ ground state to the final 1^- state of ^{6}He. We have investigated the detailed structure of the $E1$ (dipole) strength distribution from two perspectives, the first is to fix the pairing strength and the second is to study the role of different configurations. Figure 7, shows the total dipole transition strength of ^{6}He with different values of G and table 4 tabulates the total $B(E1)$ strength in e^2fm^2 with pairing strength G. As it should, it remains practically constant. The shape and strength of our dipole response function are consistent with the previous calculations [38, 52–54], although these previous studies available in the literature for the calculation of $B(E1)$ differ in the approach used. Reference [38] studies the electric dipole ($E1$) response of ^{6}He with a fully microscopic six-body calculation, ref. [52] used the complex scaling method (CSM), ref. [53] uses the R-matrix approach, whereas ref. [54] uses the pseudostate method. As a result of the smoothing procedure, the curves in fig. 7 show a few minor wiggles, that are not to be attributed to resonances, but must be considered as an artifact. It is clear, though, that there is an accumulation of strength at energies of 2–10 MeV and possibly a shallow maximum around 3–5 MeV. We find in these calculations that the transition from $[p_{3/2} \times p_{3/2}]^{(0)} \rightarrow [p_{3/2} \times d_{5/2}]^{(1)}$ plays the dominant role in total dipole transition strength, whereas all the remaining nine transitions are less significant. However, our model does not include the recoil correction at the moment. This has been discussed in ref. [55], where it is concluded that the no-recoil approximation works quite well for several observables. This correction would be important, when one includes the s-state continuum and calculate the dipole strength [47] and the $B(E1)$ strength dis-

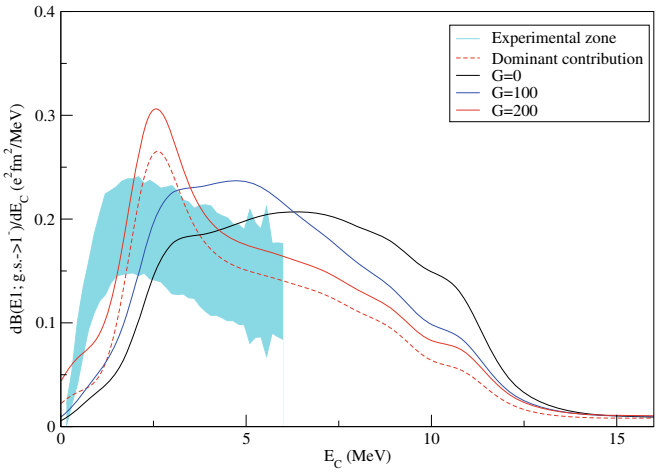

Fig. 7. (Color online) Dipole $E1$ transition strength distribution from the ground state 0^+ to the final state 1^- for ^{6}He for a few values of the pairing strength compared to experimental data up to 6 MeV from ref. [9].

Table 4. Total $B(E1)$ with varying pairing strength.

G	Total $B(E1)$ $(e^2\text{fm}^2)$
0	1.8747
100	1.8736
200	1.8378

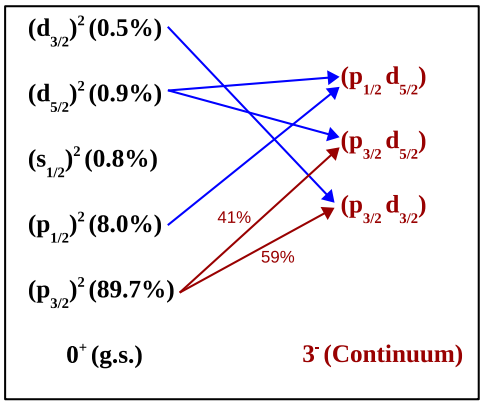

Fig. 8. (Color online) Schematic representation depicting all of the possible octupole transitions from the ground state 0^+ emerging from five different configurations to the final state 3^- emerging from three different configurations for ^{6}He. The dominant transitions are highlighted in red color along with their percentage contribution.

Table 5. Total $B(E3)$ with varying pairing strength G.

G	Total $B(E3)$ $(e^2\text{fm}^6)$
0	91.2076
250	91.1592
500	91.0861
660	90.8239

tribution would be underestimated in the absence of this correction [56]. We expect this correction to be important for the dipole only. This is probably the reason why the shape of the peak of the dipole resonance is slightly different from the experimental one.

9 Octupole strength distribution

We have also investigated the detailed structure of the $E3$ (octupole) strength distribution of the system. After constructing a basis of dimensions $N = 50$, made up of three parts, namely $[p_{1/2} \times d_{5/2}]^{(3)}$, $[p_{3/2} \times d_{3/2}]^{(3)}$ and $[p_{3/2} \times d_{5/2}]^{(3)}$, we diagonalize the pairing matrix and obtain the eigenvalues, that are all unbound, and the corresponding eigenvectors. We did calculations for four different values of the pairing strength G_3, *i.e.* 0, 250, 500 and 660 (upper limit to get all states unbound). From fig. 8, it is clear that there is a total of 6 different transitions from the initial 0^+ ground state to the final continuum 3^- state of ^{6}He. We cannot integrate to find the total strength, because we cannot extend the calculations beyond the present energy range due to computational limitations. Therefore it is not clear, at present, if we have reached the maximum value for the octupole distribution. Ideally, one should use a larger energy cut and maybe a smaller density of states. Table 5 tabulates the total $B(E3)$ strength in $e^2\text{fm}^6$ with pairing strength G up to the limit of 660. We have estimated the total octupole strength to be approximately 190 $e^2\text{fm}^6$ by following the procedure outlined in ref. [57]. Therefore our results exhaust about 50% of the total expected strength. Figure 9 shows the total octupole

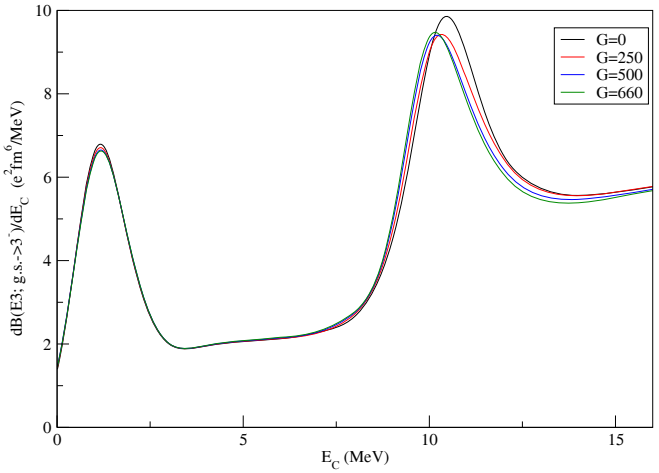

Fig. 9. (Color online) Octupole $E3$ transition strength distribution from the ground state 0^+ to the final state 3^- for ^{6}He.

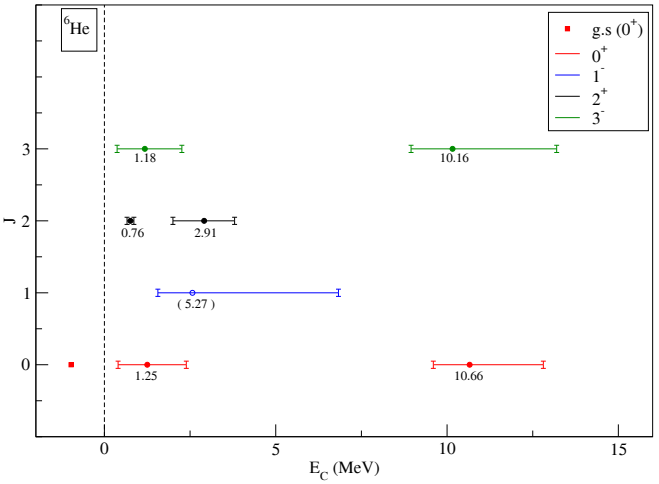

Fig. 10. (Color online) Schematic representation of the spectrum of ^{6}He predicted by our simple model. The parenthesis in the $J = 1^-$ response indicates the uncertainty on the position of the peak (see text). The lines correspond to the widths.

transition strength of ^{6}He with different values of G. The shape of our octupole response function clearly shows two large structures around 1 MeV and 10 MeV respectively, but the precise value of G has, in this case, little influence on the overall shape. This is due to the fact that with increasing l the integral between different sets of single-particle wave functions becomes progressively small and pairing becomes a weak perturbation. We have found in these calculations that both these peaks take contribution from the transitions $[p_{3/2} \times p_{3/2}]^{(0)} \rightarrow [p_{3/2} \times d_{3/2}]^{(3)}$ and $[p_{3/2} \times p_{3/2}]^{(0)} \rightarrow [p_{3/2} \times d_{5/2}]^{(3)}$. These dominate the total octupole transition strength, amounting to approximately $\sim 59\%$ and $\sim 41\%$. All the remaining four transitions depicted in fig. 8 are comparatively less significant.

10 Conclusions

In summary, the electric multipole response of ^{6}He has been investigated by using a simple structure model [40,

43,44,46], and the role of different configurations has been explored in each case. Figure 10 shows our predictions for the response of ^{6}He to electromagnetic excitations of different multipolarity by showing the centroid of each state and the width on horizontal scale. We have computed the $B(E0)$ values (fig. 5) from the ground state to the continuum eigenstates and we have adjusted the strength of the pairing matrix to get the ground energy at the right place. We have found two peaks at energies 1.25 and 10.66 MeV. Their widths are about 1.99 and 3.21 MeV, respectively. For the dipole strength distribution (fig. 7) we have indicated in the figure the case with maximal pairing strength that shows a maximum at 2.57 MeV with an asymmetric width of 5.27 MeV. For the quadrupole strength distribution (fig. 9) we have already reported in our previous calculation [40] about the details of two resonances. Finally, for the octupole strength distribution we have found two broad structures at 1.18 and 10.16 MeV with asymmetric widths of 1.89 and 4.25 MeV, respectively. We expect that our efforts might be of help to unravel the complex patterns seen in the continuum spectrum of ^{6}He.

We would like to thank J.A. Lay, K. Hagino, Sukhjeet Singh and Antonio Moro for useful suggestions. JS gratefully acknowledges the financial support from Fondazione Cassa di Risparmio di Padova e Rovigo (CARIPARO).

References

1. I. Tanihata, H. Hamagaki, O. Hashimoto, Y. Shida, N. Yoshikawa, K. Sugimoto, O. Yamakawa, T. Kobayashi, N. Takahashi, Phys. Rev. Lett. **55**, 2676 (1985).
2. I. Tanihata *et al.*, Phys. Lett. B **160**, 380 (1985).
3. I. Tanihata *et al.*, Phys. Lett. B **206**, 592 (1985).
4. K. Tanaka *et al.*, Phys. Rev. Lett. **104**, 062701 (2010).
5. M.V. Zhukov, B.V. Danilin, D.V. Fedorov, J.M. Bang, I.J. Thompson, J.S. Vaagen, Phys. Rep. **231**, 151 (1993).
6. T. Otsuka, R. Fujimoto, Y. Utsuno, B.A. Brown, M. Honma, T. Mizusaki, Phys. Rev. Lett. **87**, 082502 (2001).
7. T. Kobayashi *et al.*, Phys. Rev. Lett. **60**, 2599 (1988).
8. N. Fukuda *et al.*, Phys. Rev. C **70**, 054606 (2004).
9. T. Aumann *et al.*, Phys. Rev. C **59**, 1252 (1999).
10. T. Nakamura *et al.*, Phys. Rev. Lett. **96**, 252502 (2006).
11. F. Catara, C.H. Dasso, A. Vitturi, Nucl. Phys. A **602**, 181 (1996).
12. F.P. Brady *et al.*, J. Phys. G **10**, 363 (1984).
13. F. Ajzenberg-Selove, Nucl. Phys. A **490**, 1 (1988).
14. J. Jänecke *et al.*, Phys. Rev. C **54**, 1070 (1996).
15. S. Nakayama *et al.*, Phys. Rev. Lett. **85**, 262 (2000).
16. T. Nakamura *et al.*, Phys. Lett. B **493**, 209 (2000).
17. X. Mougeot *et al.*, Phys. Lett. B **718**, 441 (2012).
18. O.M. Povoroznyk, V.S. Vasilevsky, Ukr. J. Phys. **60**, 3 (2015).
19. S. Nakayama *et al.*, Phys. Rev. Lett. **87**, 122502 (2001).
20. T. Nakamura, Eur. Phys. J. A **13**, 33 (2002).
21. H. Akimune *et al.*, Phys. Rev. C **67**, 051302(R) (2003).
22. S. Aoyama, S. Mukai, K. Kato, K. Ikeda, Prog. Theor. Phys. **93**, 99 (1995).
23. S. Aoyama, S. Mukai, K. Kato, K. Ikeda, Prog. Theor. Phys. **94**, 343 (1995).
24. T. Myo, S. Aoyama, K. Kato, K. Ikeda, Phys. Rev. C **63**, 054313 (2001).
25. A. Csoto, Phys. Rev. C **48**, 165 (1993).
26. K. Arai, Y. Suzuki, R.G. Lovas, Phys. Rev. C **59**, 1432 (1999).
27. N. Michel, W. Nazarewicz, M. Ploszajczak, K. Bennaceur, Phys. Rev. Lett. **89**, 042502 (2002).
28. N. Michel, W. Nazarewicz, M. Ploszajczak, K. Bennaceur, Phys. Rev. C **67**, 054311 (2003).
29. G. Hagen, M. Hjorth-Jensen, J.S. Vaagen, Phys. Rev. C **71**, 044314 (2005).
30. N. Michel, W. Nazarewicz, M. Ploszajczak, Phys. Rev. C **82**, 044315 (2010).
31. A. Volya, V. Zelevinsky, Phys. Rev. Lett. **94**, 052501 (2005).
32. T. Myo, K. Kato, K. Ikeda, Phys. Rev. C **76**, 054309 (2007).
33. S.C. Pieper, R.B. Wiringa, J. Carlson, Phys. Rev. C **70**, 054325 (2004).
34. P. Navrátil, W.E. Ormand, Phys. Rev. C **68**, 034305 (2003).
35. P. Navrátil, J.P. Vary, W.E. Ormand, B.R. Barrett, Phys. Rev. Lett. **87**, 172502 (2001).
36. B.V. Danilin, T. Rogde, S.N. Ershov, H. Heiberg-Andersen, J.S. Vaagen, I.J. Thompson, M.V. Zhukov, Phys. Rev. C **55**, R577 (1997).
37. B.V. Danilin, I.J. Thompson, J.S. Vaagen, M.V. Zhukov, Nucl. Phys. A **632**, 383 (1998).
38. D. Mikami, W. Horiuchi, Y. Suzuki, Phys. Rev. C **89**, 064303 (2014).
39. C. Romero-Redondo, S. Quaglioni, P. Navrátil, G. Hupin, Phys. Rev. Lett. **113**, 032503 (2014).
40. L. Fortunato, R. Chatterjee, Jagjit Singh, A. Vitturi, Phys. Rev. **90**, 064301 (2014).
41. N. Austern, Y. Iseri, M. Kamimura, M. Kawai, G.H. Rawitscher, M. Yahiro, Phys. Rep. **154**, 125 (1987).
42. R.A.D. Piyadasa, M. Kawai, M. Kamimura, M. Yahiro, Phys. Rev. C **60**, 044611 (1999).
43. Jagjit Singh, L. Fortunato, Acta Phys. Pol. B **47**, 833 (2016).
44. Jagjit Singh, PhD Thesis, University of Padova, Italy (2016).
45. TUNL, Nuclear Data Evaluation, `http://www.tunl.duke.edu/NuclData/General_Tables/5he.shtml`.
46. Jagjit Singh, AIP Conf. Proc. **1681**, 020009 (2015).
47. K. Hagino, H. Sagawa, Phys. Rev. C **72**, 044321 (2005).
48. T. Myo *et al.*, Prog. Part. Nucl. Phys. **79**, 1 (2014).
49. G.F. Bertsch, H. Esbensen, Ann. Phys. (N.Y.) **209**, 327 (1991).
50. J. Kantele, Nucl. Instrum. Methods A **271**, 625 (1988).
51. J. Meyer, P. Quentin, M. Brack, Phys. Lett. B **133**, 279 (1983).
52. S. Aoyama, S. Mukai, K. Kato, K. Ikeda, Prog. Theor. Phys. **116**, 1 (2006).
53. P. Descouvemont, E. Pinilla, D. Baye, Prog. Theor. Phys. Suppl. **196**, 1 (2012).
54. J.A. Lay, A.M. Moro, J.M. Arias, J. Gómez-Camacho, Phys. Rev. C **82**, 024605 (2010).
55. H. Esbensen, G.F. Bertsch, K. Hencken, Phys. Rev. C **56**, 3054 (1997).
56. H. Sagawam K. Hagino, Eur. Phys. J. A **51**, 102 (2015).
57. H. Sagawa, N. Takigawa, Nguyen van Giai, Nucl. Phys. A **543**, 575 (1992).